

Article

Detection of Aquatic Plants Using Multispectral UAV Imagery and Vegetation Index

Bonggeun Song¹ and Kyunghun Park^{2,*}

¹ Institute of Industrial Technology, Changwon National University, Changwon, Gyeongsangnam-do 641-773, Korea; envsong@changwon.ac.kr

² School of Civil, Environmental and Chemical Engineering, Changwon National University, Changwon, Gyeongsangnam-do 641-773, Korea

* Correspondence: landpkh@changwon.ac.kr; Tel.: +82-10-9992-7567; Fax: +82-55-281-3011

Received: 27 November 2019; Accepted: 22 January 2020; Published: 25 January 2020



Abstract: In this study, aquatic plants in a small reservoir were detected using multispectral UAV (Unmanned Aerial Vehicle) imagery and various vegetation indices. A Firefly UAV, which has both fixed-wing and rotary-wing flight modes, was flown over the study site four times. A RedEdge camera was mounted on the UAV to acquire multispectral images. These images were used to analyze the NDVI (Normalized Difference Vegetation Index), ENDVI (Enhance Normalized Difference Vegetation Index), NDREI (Normalized Difference RedEdge Index), NGRDI (Normalized Green-Red Difference Index), and GNDVI (Green Normalized Difference Vegetation Index). As for multispectral characteristics, waterside plants showed the highest reflectance in R_{nir} , while floating plants had a higher reflectance in R_{re} . During the hottest season (on 25 June), the vegetation indices were the highest, and the habitat expanded near the edge of the reservoir. Among the vegetation indices, NDVI was the highest and NGRDI was the lowest. In particular, NGRDI had a higher value on the water surface and was not useful for detecting aquatic plants. NDVI and GNDVI, which showed the clearest difference between aquatic plants and water surface, were determined to be the most effective vegetation indices for detecting aquatic plants. Accordingly, the vegetation indices using multispectral UAV imagery turned out to be effective for detecting aquatic plants. A further study will be accompanied by a field survey in order to acquire and analyze more accurate imagery information.

Keywords: unmanned aircraft vehicle; remote sensing; vegetation index; aquatic plants; GIS; multi-spectral

1. Introduction

It is widely known that aquatic plants in water bodies such as rivers and reservoirs can improve water quality [1–3]. In particular, floating plants live on the water surface rather than rooting in soil; as their leaves and stems float on the water surface, floating plants block light penetration, hinder the photosynthesis of phytoplankton, and reduce the concentration of chlorophyll-a, thereby suppressing green algae [4]. Recently, the ability of aquatic plants to improve water quality has been utilized to purify polluted rivers or reservoirs from an ecological perspective [5], and various studies are being conducted to investigate the distribution of aquatic plants living in water.

Field surveys have been the conventional method for identifying vegetation. The salient advantage of this method is the careful observation of plant species. However, if a large area is investigated, then field surveys require a large amount of labor, cost, and time [6,7]. In particular, as aquatic plants often live in inaccessible regions, direct field surveys are not as effective as expected.

Recently, the remote sensing method, which uses satellite images or UAVs (unmanned aerial vehicles) to survey and monitor vegetation in a target area, has been actively adopted instead of field

surveys. As satellites can periodically provide imagery while moving in an orbit, they are very useful for analyzing patterns of ecosystem change [8,9]. Furthermore, a wide area stretching from a few meters to kilometers can be analyzed within a short time [10]. Nevertheless, as most satellite images have a middle or low spatial resolution, they are not sufficient for the precise analysis of plant species or small-scale ecosystems [11–13]. To solve this problem, UAVs are actively used for surveys [14,15]. Since UAVs are operated at lower altitudes than satellites, higher resolution images can be acquired [16,17], enabling plant species or habitats to be precisely analyzed [18,19]. Moreover, UAVs can be operated to freely acquire information about any area at any time desired, and can be effectively used to monitor inaccessible regions, for which satellite imagery cannot be acquired; additionally, they can identify the impact of environmental factors like heavy rainfall, snowfall, and heat waves [20].

Vegetation surveys using UAVs mainly obtain high resolution images and analyze the unique spectral information of plants to classify plant species or identify the distribution of habitats [7,13,16,21–24]. For such an analysis, a vegetation index (VI) is usually applied, which is derived from the characteristics of various spectral wavelengths [25–27]. The vegetation index is an indicator that quantifies the presence or absence of vegetation, the greenness of land cover, or the vitality of vegetation. Currently, the vegetation index is utilized not only for monitoring plant habitats, but also in various areas including the analysis of drought and environmental change [28,29]. However, most previous studies have applied the vegetation index to inland forest or agricultural areas, whereas only a few studies have dealt with aquatic plants. This is important because, as aquatic plants float on the water surface, they may have different spectral properties than those of land plants.

This study evaluated a UAV-based method of surveying the distribution of aquatic plant habitats in a small reservoir located in Gyeongju-si, Republic of Korea. The analysis proceeded as follows: (1) multispectral UAV images were acquired and the spectral characteristics for aquatic plants and water surface were analyzed, and (2) various vegetation indices used in the existing studies were analyzed to see what method was appropriate for surveying the habitats of aquatic plants.

2. Materials and Methods

2.1. Study Reservoir

This study was conducted for the region of Hayeombulji (N35.801, E129.186), located in Gyeongju-si, Gyeongsangbuk-do, Republic of Korea (Figure 1). Hayeombulji has an area of 47.103 m², a diameter of about 230 m, and a depth of 4 ~ 5 m [30]. With regard to the climate, the reservoir has four distinct seasons. In the summer, during which a large amount of agricultural activity takes place, the temperature reaches up to approximately 30 °C, and the reservoir water is extensively used for agriculture. Accordingly, aquatic plant habitats need to be analyzed in order to ensure a supply of clean water for agricultural purposes.

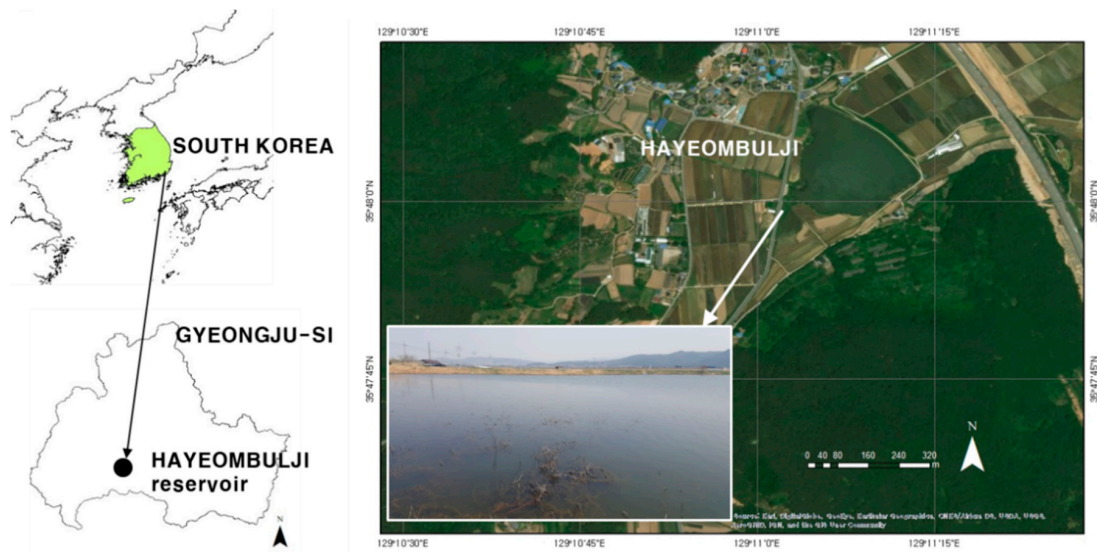


Figure 1. Study area.

2.2. UAV Imagery Acquisition and Processing

In this study, a RedEdge multispectral camera from MicaSense was mounted on a Firefly to obtain UAV imagery (Figure 2). The Firefly uses both rotary-wing and fixed-wing flight modes. The rotary-wing mode is adopted during the taking-off and landing phases, which enables the vertical movement of the UAV. After take-off, the UAV flies horizontally in the fixed-wing flight mode, during which imagery is acquired. Consequently, the Firefly has relatively long flight times, thereby addressing a disadvantage of rotary-wing UAVs as well as requiring relatively little space for take-off and landing, overcoming a disadvantage of fixed-wing UAVs. The MicaSense RedEdge multispectral camera (MicaSense Inc., Seattle, WA, USA) has five spectral wavelength bands (blue, green, red, near IR, RedEdge). The detailed specifications of the Firefly UAV and the MicaSense RedEdge multispectral camera are presented in Tables 1–3.



Figure 2. Firefly UAV and RedEdge multispectral camera.

Table 1. Specifications of the Firefly UAV.

Division	Contents
Flying speed	50 ~ 60 km/h
Weight	4.1 kg (included camera and battery)
Flying time	45 min
Weather condition	wind speed under 10 m/s
Elevation	10 ~ 1000 m (standard: 150 m)
Resolution	1 ~ 25 cm

Table 2. Spectral bands of the MicaSense RedEdge multispectral camera.

Band Number	Band Name	Center Wavelength (nm)	Bandwidth FWHM (nm)
1	Blue	475	20
2	Green	560	20
3	Red	668	10
4	Near IR	840	40
5	Red Edge	717	10

Source: MicaSense RedEdge Multispectral Camera User Manual.

Table 3. Specifications of the MicaSense RedEdge multispectral camera.

Specifications	
Weight	150 g
Dimensions	2.1 cm × 6.6 cm × 4.6 cm
Ground sample distance	8.2 cm/pixel (per band) at 120 m
Capture speed	1 capture per second (all bands), 12-bit RAW

Source: MicaSense RedEdge Multispectral Camera User Manual.

UAV imagery was acquired four times (25 April, 20 May, 25 June, and 24 October 2018). The flight path was set using Firefly 6 Planner, which is the dedicated software for the Firefly UAV, and considered geographic features around the study area (Figure 3). During the first flight on 25 April 2018, the flight path was set, and the UAV was operated in the same path for the remaining flights. While the UAV was operated, the duplication rate, flight time, and flight altitude were set to 80%, about 20 min, and 150 m, respectively. Before each flight, the reflectance panel was used to calibrate the reflectance of the multispectral imagery. The operation of the UAV was initiated by pressing the start button in Firefly 6 Planner. With the UAV flight, 338 images were acquired for each spectral wavelength band. Five orthoimages were fabricated in each spectral wavelength band from images obtained from the UAV by using Pix4D Software 2.1 (Pix4D: Lausanne, Switzerland, 2016). The analysis process consists of orthoimages through initial processing, point cloud, mesh generation, orthomosaic, and image correction using reflection panel information.

2.3. Analysis of UAV Imagery

2.3.1. Vegetation Index

As shown in Table 2, a total of five vegetation indices were analyzed. These indices were NDVI (normalized difference vegetation index), ENDVI (extended normalized difference vegetation index), NDREI (normalized difference red edge index), NGRDI (normalized green-red difference index), and GNDVI (green normalized difference vegetation index). Five vegetation indices were selected because they are widely used for extracting vegetation areas in previous studies and can be analyzed using the spectral wavelength bands acquired from the RedEdge M sensor. For the analysis method, the Raster Calculator Tool in ArcGIS Ver. 10.2 was applied to the orthoimages of each spectral wavelength band, as shown in Table 4.

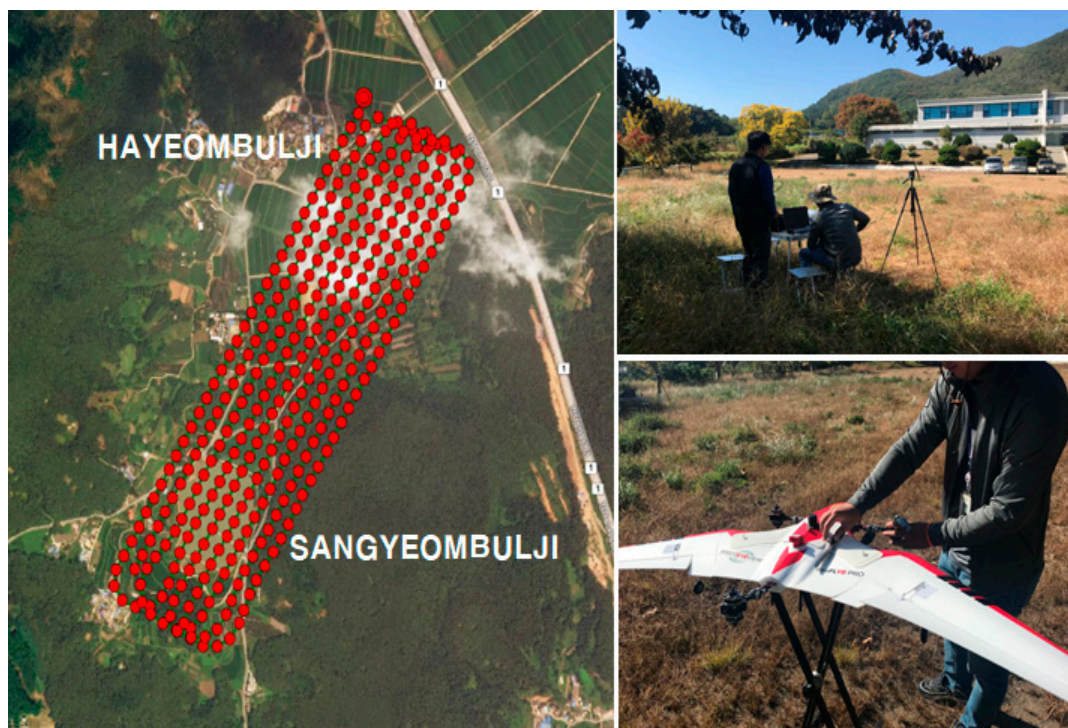


Figure 3. Flight path setting and the UAV operation using Firefly 6 Planner S/W.

Table 4. Vegetation indices using multi-spectral imagery.

Name	Abbreviation	Formula	Value Range	Reference
Blue	R_b	R_b	-	
Green	R_g	R_g	-	
Red	R_r	R_r	-	
RedEdge	R_{re}	R_{re}	-	
Near-infrared	R_{nir}	R_{nir}	-	
Normalized Difference Vegetation Index	NDVI	$(R_{nir} - R_r) / (R_{nir} + R_r)$	-1 ~ 1	[31]
Enhance Normalized Difference Vegetation Index	ENDVI	$[(R_{nir} + R_g) - (2 \times R_b)] / [(R_{nir} + R_g) + (2 \times R_b)]$	-1 ~ 1	[32]
Normalized Difference RedEdge Index	NDREI	$(R_{nir} - R_{re}) / (R_{nir} + R_{re})$	-1 ~ 1	[33]
Normalized Green-Red Difference Index	NGRDI	$(R_g - R_r) / (R_g + R_r)$	-1 ~ 1	[34]
Green NDVI	GNDVI	$(R_{nir} - R_g) / (R_{nir} + R_g)$	-1 ~ 1	[35]

2.3.2. Profile Analysis

A profile analysis was performed to identify the characteristics of spectral wavelength bands and vegetation indices with respect to the covering characteristics of water space such as aquatic plants and water surface. Polyline features were created in ArcGIS 10.2 at 1 m intervals for some sections of the study area, which included both aquatic plants and the water surface (Figure 4), while the reflectance of a spectral wavelength band and the mean vegetation index for each section were calculated using zonal statistics tools. Subsequently, the mean values were calculated for the polyline features, and the reflectance of the spectral wavelength band and the characteristics of vegetation indices were analyzed according to the presence of aquatic plants.



Figure 4. Section setting for the profile analysis.

3. Results

3.1. Spectral Characteristics of Aquatic Plants

Figure 5 illustrates the reflectance of each spectral wavelength band, which was obtained through the profile analysis. On 25 April, the closer to location A (i.e., the reservoir edge), higher reflectance was shown in every wavelength band. In particular, R_{nir} and R_{re} had a higher reflectance than the remaining wavelength bands. In the other areas, there was no significant difference in terms of reflectance among the spectral wavelength bands. In contrast to the reflectance recorded on 25 April, those recorded on both 20 May and 25 June displayed peaks in many areas. This was because the habitats of waterside plants and floating plants had expanded, which resulted in an increase of reflectance in areas including such habitats. In particular, the waterside plants had the highest reflectance in R_{nir} , while the floating plants showed a high reflectance in R_{re} . Accordingly, the waterside plants and the floating plants had different reflectance patterns in each spectral wavelength band (Figure 5a). Unlike the other spectral band, R_r and R_b did not show any significant change of reflectance. The waterside plants had a similar pattern in every wavelength band. On the other hand, the floating plants showed an increasing and decreasing pattern only in R_{nir} , R_{re} , and R_g , but displayed no significant change in R_r and R_b . As the floating plants are submerged in water or afloat on water, they tend to be much more affected by spectral reflectance and thus may show a different characteristic of reflectance in each spectral wavelength band from the waterside plants that are not submerged in water. Consequently, the reflectance characteristics in each spectral wavelength band were clearly different according to the type of aquatic plants and habitats. Moreover, among the aquatic plants, the floating plants and the waterside plants showed a significant difference in terms of reflectance in each spectral wavelength band according to habitat.

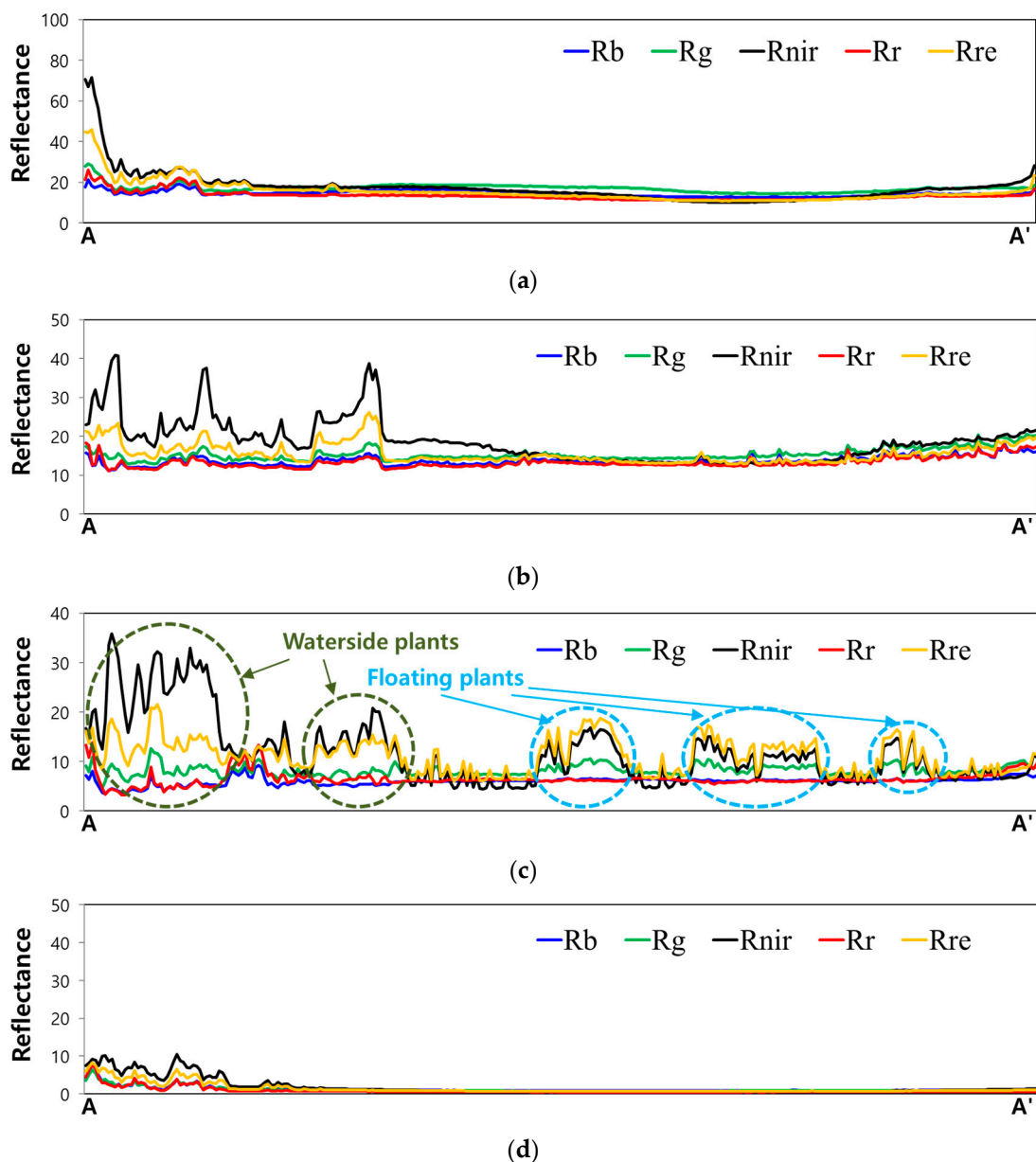


Figure 5. Profile analysis results for each spectral wavelength band. (a) 04/25/2018; (b) 05/20/2018; (c) 06/25/2018; (d) 10/24/2018.

3.2. Results of Vegetation Index Analysis

Figure 6 presents the analysis results of various vegetation indices. The mean values of the vegetation indices were lowest on April 25 (NDVI: 0.139, ENDVI: 0.095, NDREI: 0.086, NGRDI: 0.123, GNDVI: 0.017), but highest on June 25 (NDVI: 0.820, ENDVI: 0.368, NDREI: 0.164, NGRDI: 0.198, GNDVI: 0.222) (Figure 7). This indicates that the aquatic plants drastically proliferated for about two months. South Korea has hot summer days in June, where the highest temperature reaches up to approximately 30 °C and plants proliferate; the aquatic plants of the reservoir followed this trend, and vegetation indices seemed to be highest in this season. The areas with a vegetation index of 0.4 or above tended to gradually expand from the edge to the interior of the reservoir, indicating that the habitats of aquatic plants spread in the same direction. In comparison to that in June, the vegetation indices recorded on October 24 drastically decreased; this corresponded with the gradual temperature decrease in fall (NDVI: 0.388, ENDVI: 0.361, NDREI: 0.148, NGRDI: 0.200, GNDVI: 0.203).

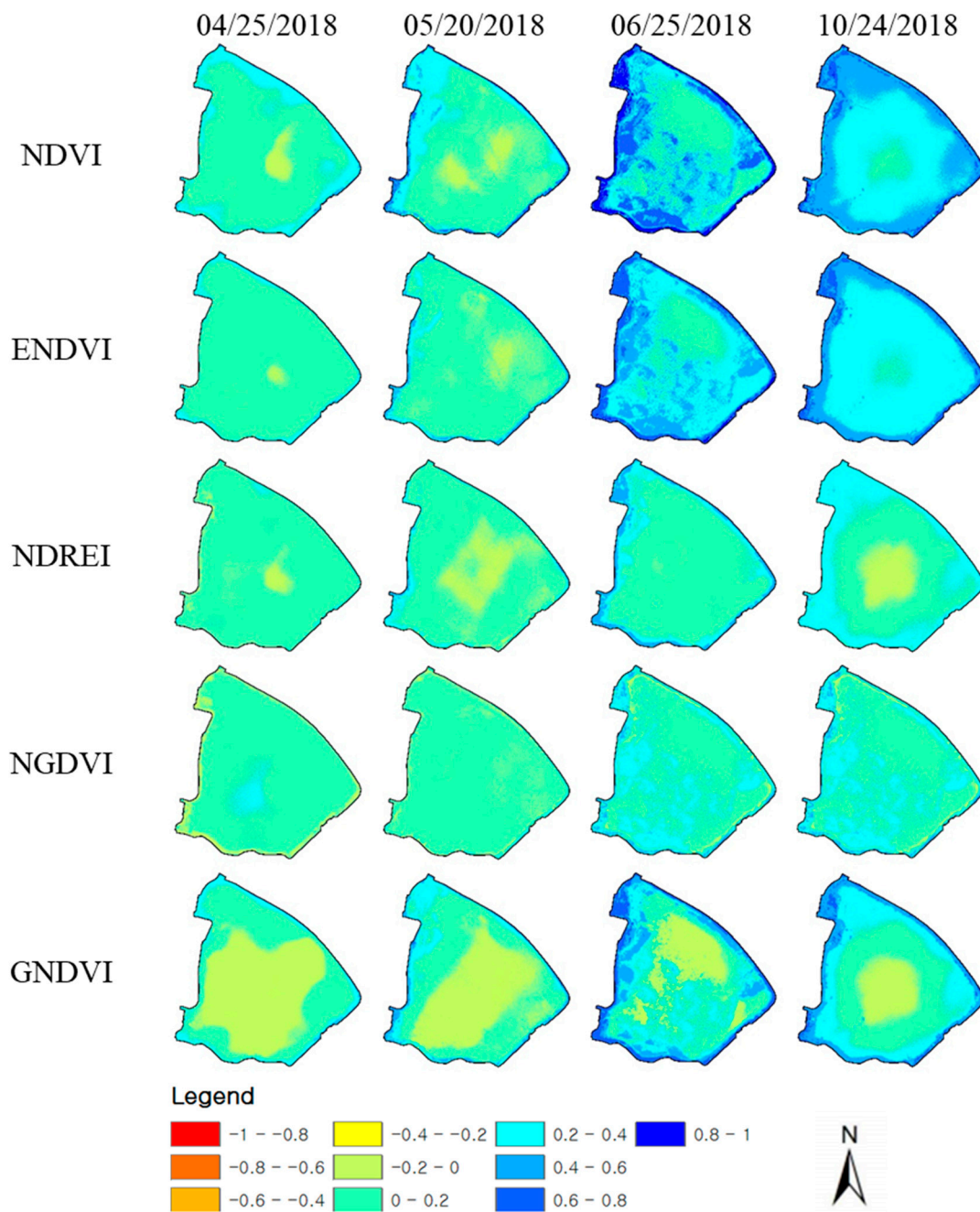


Figure 6. Analysis results of the vegetation indices.

Regarding the trends of each vegetation index, the mean values changed by only about 0.1 from April 25 (NDVI: 0.139, ENDVI: 0.095, NDREI: 0.086, NGRDI: 0.123, GNDVI: 0.017) to May 20 (NDVI: 0.140, ENDVI: 0.101, NDREI: 0.076, NGRDI: 0.072, GNDVI: 0.071). However, on June 25, the NDVI and the other vegetation indices (ENDVI: 0.451, NDREI: 0.656, NGRDI: 0.622, GNDVI: 0.598) displayed a significant difference. The NDVI was calculated by using R_{nir} and R_r . As is clear from Figure 5, the aquatic plants had the highest reflectance in R_{nir} and the lowest one in R_r . In other words, the difference in terms of reflectance was largest between these two wavelength bands. Accordingly, the NDVI was higher than any other vegetation indices.

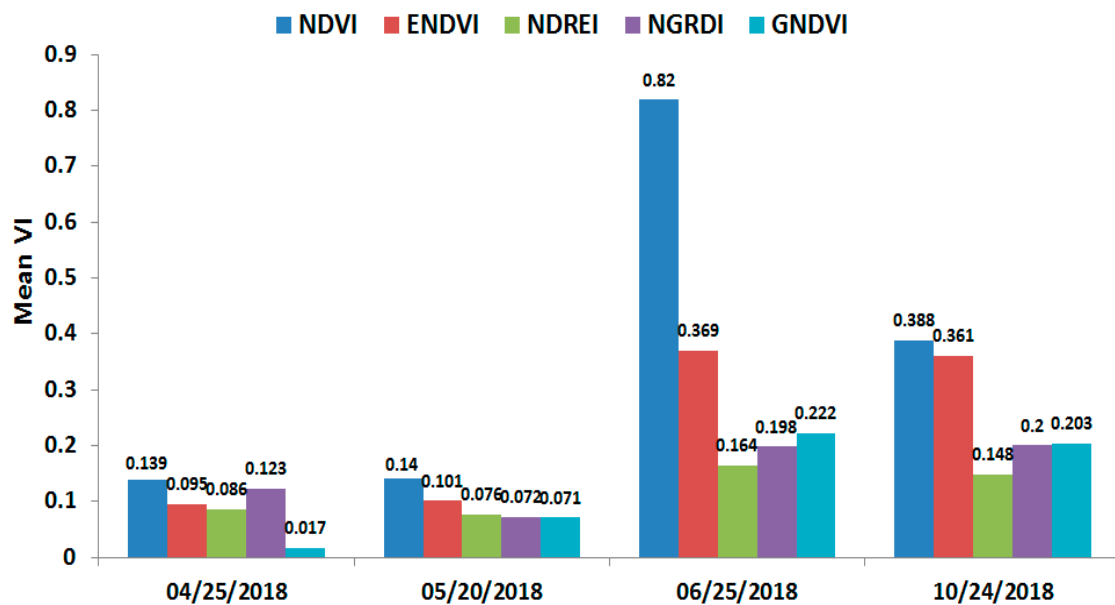


Figure 7. Mean values of the vegetation indices on each day.

On the other hand, the GNDVI and NDREI were low. On April 25 and on May 20, when the aquatic plants had not yet proliferated, GNDVI was the lowest (0.017 on April 25, 0.071 on May 20). On June 25 and on October 24, when the aquatic plants had proliferated, NDREI was the lowest (0.164 on June 25, 0.148 on October 24). The GNDVI was calculated based on R_{nir} and R_g . As the difference between R_{nir} and R_g was larger than the one between R_{nir} and R_{re} , which are used to calculate NDREI, the GNDVI was greater than the NDREI. As shown in Figure 6, most parts of the reservoir had a GNDVI of -0.2 or below on April 25 and on May 20. On the other hand, NDREI was between -0.2 and 0 over a large area. Accordingly, the mean value of the GNDVI was lower than that of NDREI. On June 25 and on October 24, many parts of the reservoir had a GNDVI of 0.4 or above, while only the reservoir edge had an increased NDREI, although the other areas did not.

Consequently, the vegetation indices had different trends according to the proliferation time of aquatic plants. This seems to be because of the characteristics of spectral wavelength bands, which were used to calculate the vegetation indices. Thus, such characteristics of spectral wavelength bands and vegetation indices need to be carefully analyzed and utilized in order to detect aquatic plants.

3.3. Characteristics of Aquatic Plant Vegetation Indices

Figure 8 presents the profile analysis results for each season and vegetation index. Generally, the vegetation indices had different trends according to the season. In areas where aquatic plants were detected, the NDVI was the highest, followed by the ENDVI and GNDVI. On April 25 and on May 20, the GNDVI was higher than the ENDVI. In contrast, on June 25 and on October 24, the ENDVI was higher than the GNDVI. The NGRDI of aquatic plants was low, but nevertheless higher than the NDVI, ENDVI, and GNDVI on the water surface. As shown in Figure 5, the reflectance did not significantly vary among the wavelength bands on the water surface. However, since the aquatic plants had a high reflectance in R_{nir} and R_{re} , the NGRDI, which is calculated using R_g and R_r , was low in the aquatic plants, but high on the water surface.

Similar to the previously described analysis results, the vegetation indices were the highest on June 25 (NDVI: 0.448, ENDVI: 0.414, NDREI: 0.178, NGRDI: 0.209, GNDVI: 0.285). In particular, the NDVI, ENDVI, and GNDVI showed a significant difference from the values recorded on April 25, when the aquatic plants had not yet proliferated (NDVI: 0.334, ENDVI: 0.339, NDREI: 0.130, NGRDI: 0.086, GNDVI: 0.304). Additionally, for areas where floating plants appeared and where the vegetation indices on the water surface had been low, the indices recorded on June 25 were high (Figure 8c).

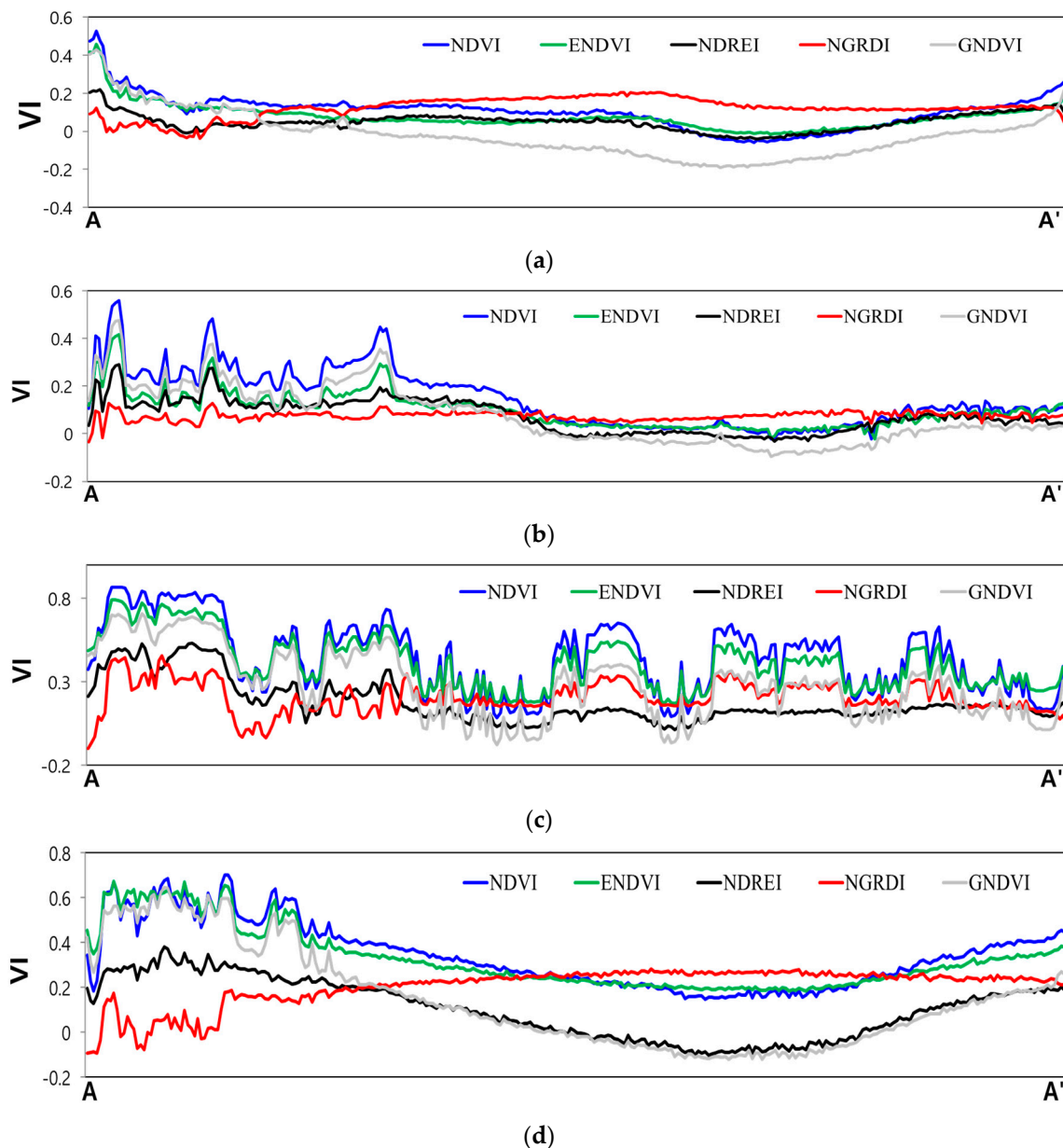


Figure 8. Profile analysis results of each vegetation index on each day. (a) 25 April 2018; (b) 20 May 2018; (c) 25 June 2018; (d) 24 October 2018.

A statistical analysis was performed to derive a vegetation index that could be used to detect aquatic plants, as shown in Table 5. The determination of an appropriate vegetation index was based on the fact that the difference of the vegetation index between the aquatic plant and the water surface increased along with the standard deviation of the index. In fact, the NDVI (0.091 on April 25, 0.122 on May 20, 0.211 on June 25, 0.145 on October 24) and GNDVI (0.122 on April 25, 0.123 on May 20, 0.207 on June 25, 0.221 on October 24) had a larger standard deviation than the other vegetation indices. Accordingly, NDVI and GNDVI seemed to be more effective than the other indices for detecting aquatic plants.

Table 5. Profile analysis result: mean value, maximum and minimum values, and standard deviation (S.D.) of each vegetation index.

Date		NDVI	ENDVI	NDREI	NGRDI	GNDVI
25 April 2018	Mean	0.104	0.075	0.048	0.123	−0.019
	Max.	0.526	0.459	0.218	0.206	0.431
	Min.	0.059	−0.015	−0.040	−0.037	−0.019
	S.D.	0.091	0.067	0.047	0.053	0.122
20 May 2018	Mean	0.147	0.099	0.074	0.075	0.075
	Max.	0.558	0.417	0.291	0.128	0.476
	Min.	−0.023	−0.021	−0.033	−0.035	−0.095
	S.D.	0.122	0.076	0.069	0.018	0.123
25 June 2018	Mean	0.448	0.414	0.178	0.209	0.285
	Max.	0.868	0.792	0.533	0.458	0.709
	Min.	0.084	0.170	0.014	−0.101	−0.077
	S.D.	0.211	0.163	0.128	0.095	0.207
24 October 2018	Mean	0.342	0.327	0.103	0.203	0.147
	Max.	0.701	0.672	0.380	0.282	0.645
	Min.	0.147	0.183	−0.104	−0.094	−0.122
	S.D.	0.145	0.136	0.103	0.085	0.221

When the NDVI and GNDVI were compared with each other in detail, there was no significant difference between the NDVI and GNDVI in different habitats on April 25. However, the GNDVI was lower than the NDVI by about 0.2 on the water surface. On May 20, the NDVI was higher than the GNDVI by about 0.05, but both showed a similar pattern across all habitats. However, the GNDVI was lower than the NDVI by about 0.1 on the water surface. On June 25, when the aquatic plants had proliferated, the NDVI was higher than the GNDVI by about 0.2, although both indices generally displayed a similar pattern. On 25 October, there was little difference between the vegetation indices between habitats. However, on the water surface, the GNDVI was lower than the NDVI by about 0.3; in fact, the NDVI was generally higher than the GNDVI. However, as for the difference between aquatic plants and the water surface, the GNDVI was higher than the NDVI.

Figure 9 shows the analysis results of scatter plots with the criterion of the NDVI in order to identify vegetation index trends according to the characteristics of aquatic plants and the water surface. On 25 April, all the vegetation indices were positively (+) correlated to the NDVI, with the exception of the NGRDI. In particular, the ENDVI was very highly correlated to NDVI ($R^2 = 0.9189$). The NGRDI was negatively (−) correlated to the NDVI, but the correlation was very low ($R^2 = 0.1306$). On 20 May, all the vegetation indices were positively correlated to the NDVI. However, the R^2 of the NGRDI was as low as 0.1181. On 25 June, the R^2 was at least 0.4 in every vegetation index. In particular, the GNDVI and ENDVI showed a high correlation (GNDVI = 0.9168, ENDIV = 0.9715). Like the results for 25 April, all the vegetation indices were positively (+) correlated to the NDVI on 25 October, with the exception of NGRDI.

The GNDVI, ENDVI, and NDREI were highly correlated to the NDVI and showed the same characteristics according to the covering types of the reservoir including aquatic plants and the water surface. On the other hand, the NGRDI had a low correlation to the NDVI and the negative correlation, that is, the opposite tendency was shown in all seasons except for summer (25 June), where there was a large amount of vegetation. This was because the NDVI was high in habitats, but the NGRDI was low in aquatic plants and rather high on the water surface.

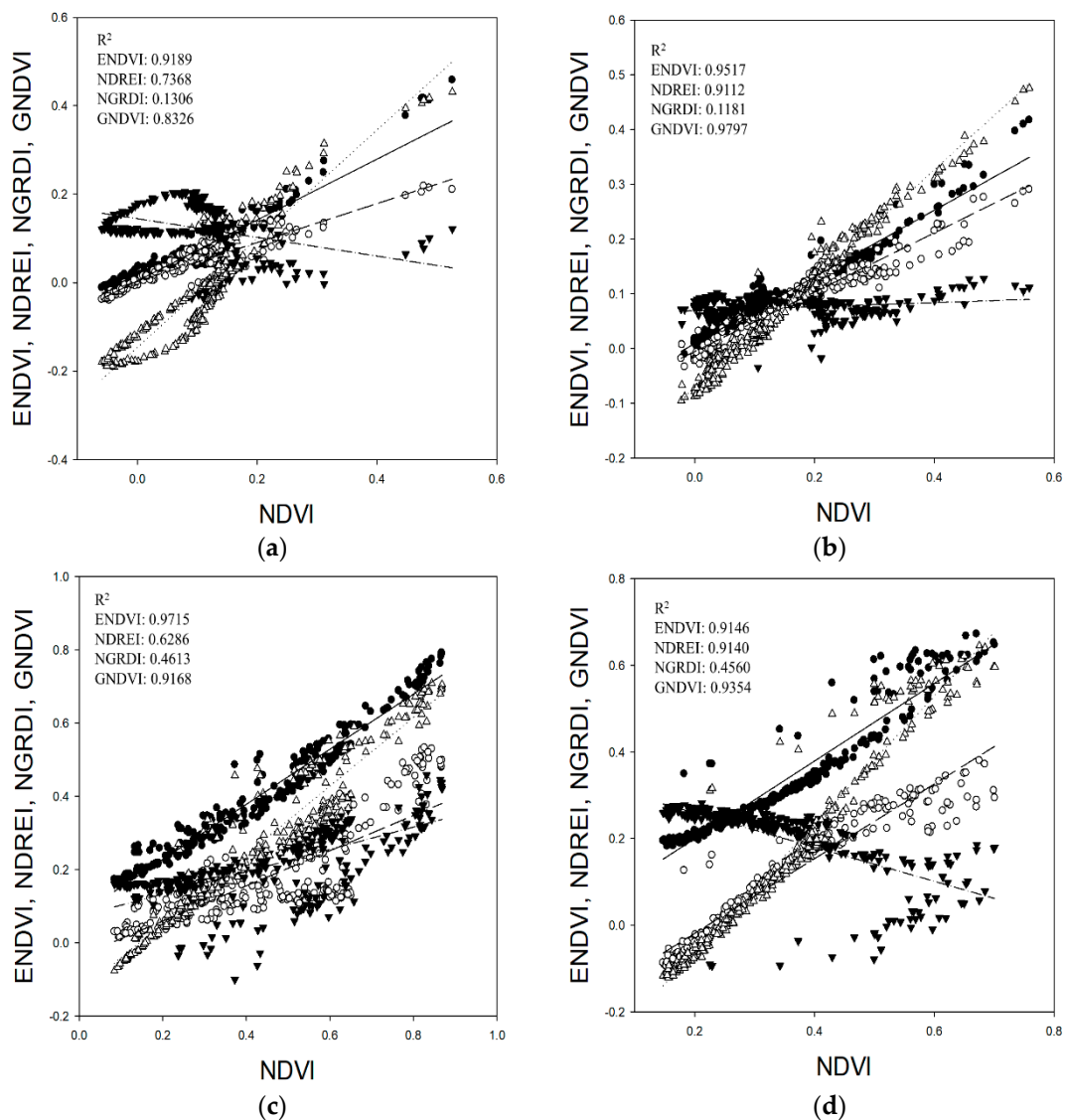


Figure 9. Results of the scatter plot analysis between the NDVI and each vegetation index (ENDVI, NDREI, NGRDI, GNDVI) (●: ENDVI, ○: NDREI, ▼: NGRDI, △: GNDVI). (a) 25 April 2018; (b) 20 May 2018; (c) 25 June 2018; (d) 24 October 2018.

4. Discussion

As a result of analyzing the characteristics of aquatic plants for various vegetation indices extracted by multispectral UAV imagery, all vegetation indices except the NGRDI showed a similar tendency, according to the presence or absence of aquatic plants. Among the existing studies using the NGRDI, [36] calculated the NGRDI by utilizing the UAV imagery information and analyzed the correlation between the biomass on the ground surface and the leaf area index (LAI). They reported that the correlation coefficient (r) between the NGRDI and biomass was 0.54 ~ 0.78; furthermore, the NGRDI from UAV imagery was cost-effective in predicting biomass. Additionally, [37] reported that the NGRDI was more effective than NDVI in extracting N fertilization. Furthermore, [38] revealed that NGRDI was effective in detecting green algae and biomass. Rasmussen et al. [25], Smigaj et al. [39], Shimada et al. [40], and Li et al. [41] also utilized the NGRDI to detect fertilizer or biomass in agricultural regions. As shown in the existing studies, since the NGRDI is derived by using the spectral wavelength bands of R_r and R_g , it seems to be effective in detecting green algae or analyzing the characteristics of plants in summer, where leaves are green due to the high vitality of plants.

However, R_r and R_g did not have a significant difference with regard to the reflectance between aquatic plants and the water surface. Accordingly, the NGRDI does not seem to be appropriate for detecting aquatic plants.

Among the vegetation indices, except the NGRDI, the most effective vegetation indices of the aquatic plant areas were the NDVI and GNDVI. The NDVI and GNDVI were clearly distinguished as their values were most significantly different between aquatic plants and the water surface (Figure 8). As shown in Figure 10, in order to see whether the NDVI and GNDVI can be used to detect aquatic plants, the NDVI and GNDVI were set to a specific value or above (NDVI: 0.35 or above, GNDVI: 0.25 or above) on 25 June when aquatic plants had proliferated, and the habitats of aquatic plants were extracted. In comparison with the RGB images, the distribution of habitats thus extracted was similar to the real distribution of aquatic plants, although there was a difference with regard to the aquatic plant area (i.e., area B). Additionally, the area of aquatic plant by the NDVI was found to be larger than that of the GNDVI (NDVI: 356.63 m², GNDVI: 269.06 m²).

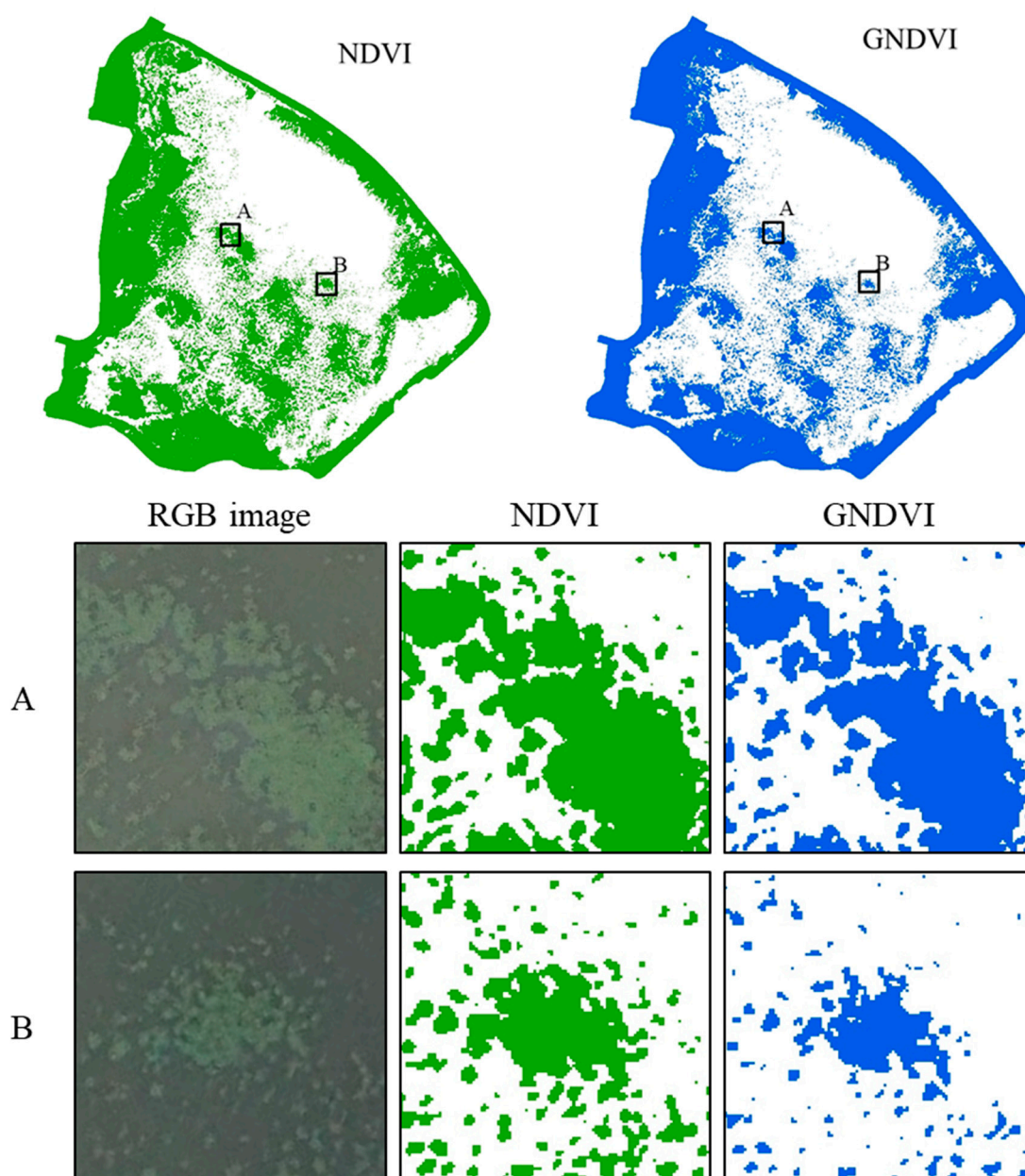


Figure 10. Extracted habitats of aquatic plants using the NDVI and GNDVI on June 25.

These results show that it is difficult to identify which vegetation indices are more effective in detecting aquatic plant areas. This is because the aquatic plant area in the reservoir is unknown accurately. However, the vegetation indices extracted from the UAV, which has been used for forest ecosystems, can be used to monitor the habitat change of aquatic ecosystems in high resolution. In addition, more accurate vegetation index values need to be applied in order to extract aquatic plant areas. Additionally, the vegetation index value, according to the species of aquatic plants, should be identified, which will need to be studied continuously in the future.

5. Conclusions

This study analyzed a method of detecting aquatic plants by utilizing multispectral UAV imagery and various vegetation indices for a small reservoir. The results of this study can be summarized as follows.

The vegetation indices were highest on 25 June, which corresponded to the hottest season, and lowest on 25 April. The seasonal change of vegetation indices revealed that the habitats of aquatic plants gradually expanded from the edge of the reservoir. When the vegetation indices were compared, the NDVI had the highest mean value of 0.820 on 25 June, and the difference in relation to the remaining vegetation indices was as large as approximately 0.2 ~ 0.4. On the other days, the NDVI was also the highest, but the difference between the NDVI and the remaining indices was only about 0.1. This is attributable to the reflectance characteristics of each spectral wavelength band. In other words, the NDVI is calculated by using R_{nir} and R_r , which have the largest difference in regard to reflectance. On the other hand, the GNDVI and NDREI belonged to the lowest group. The GNDVI was lowest on 25 April and on 20 May, when aquatic plants had not yet proliferated. The NDREI was lowest on 25 June, when aquatic plants had proliferated.

The profile analysis showed that the NDVI and GNDVI were effective for detecting aquatic plants since these indices had a larger deviation than the other indices. In addition, the NDVI and GNDVI had a similar tendency according to the covering characteristics of the reservoir. However, GNDVI was much lower than the NDVI on the water surface, indicating a clearer difference between the aquatic plants and the water surface. Except on 25 June, the GNDVI was similar to the NDVI in aquatic plants, but was much lower than the NDVI on the water surface.

Accordingly, for the UAV-based detection of aquatic plants, the GNDVI seems to be effective along with the NDVI, which has been widely applied in previous studies. However, when the habitats of aquatic plants are extracted using the NDVI and GNDVI, accurate vegetation index values of aquatic plants need to be identified. Although this study analyzed the characteristics of spectral information regarding aquatic plants using multispectral imagery, a field survey for verification and calibration is also necessary for the more accurate identification of spectral characteristics.

This study has demonstrated that UAV imagery is sufficiently applicable for analyzing the distribution of aquatic plants. This method is costly, so the necessity of a cost-effective method for utilizing UAVs has received much attention. With this regard, the above results indicate a low cost and high effective method for detecting aquatic plants. The method proposed in this study seems to be applicable to the area of surveying aquatic plants. Of course, it is still necessary to verify the accuracy of both imagery information and analysis results through a field survey. A further study will deal with this issue and supplement the limitations of this study.

Author Contributions: B.S. and K.P. conceived and designed the research; B.S. performed the field measurements; and K.P. and B.S. analyzed the spatial data and wrote the paper. All authors have read and agreed to the published version of the manuscript.

Funding: This research was supported by the Basic Science Research Program through the National Research Foundation of Korea (NRF) funded by the Ministry of Education (No. NRF-2019R111A1A01063568) and the Korea Ministry of Environment as Waste to Energy-Recycling Human Resource Development Project (YL-WE-19-001).

Conflicts of Interest: The authors declare no conflicts of interest.

References

1. Sudiarto, S.I.A.; Renggaman, A.; Choi, H.L. Floating aquatic plants for total nitrogen and phosphorus removal from treated swine wastewater and their biomass characteristics. *J. Environ. Manag.* **2019**, *231*, 763–769. [[CrossRef](#)] [[PubMed](#)]
2. Muradov, N.; Taha, M.; Miranda, A.; Kadali, K.; Gujar, A.; Rochfort, S.; Stevenson, T.; Ball, A.S.; Mouradov, A. Dual application of duckweed and azolla plants for wastewater treatment and renewable fuels and petrochemicals production. *Biotechnol. Biofuels* **2014**, *7*, 30. [[CrossRef](#)] [[PubMed](#)]
3. Tel-Or, E.; Forni, C. Phytoremediation of hazardous toxic metals and organics by photosynthetic aquatic systems. *Plant Biosyst.* **2011**, *145*, 224–235. [[CrossRef](#)]
4. Lee, G.; Sung, K. Evaluation of the Nutrient Uptakes of Floating and Submerged Plants under Experimental Conditions. *J. Korean Soc. Water Environ.* **2012**, *28*, 71–77. (In Korean)
5. Favas, P.J.C.; Pratas, J.; Rodrigues, N.; D'Souza, R.; Varun, M.; Paul, M.S. Metal(loid) accumulation in aquatic plants of a mining area: Potential for water quality biomonitoring and biogeochemical prospecting. *Chemosphere* **2018**, *194*, 158–170. [[CrossRef](#)] [[PubMed](#)]
6. Baxendale, C.L.; Ostle, N.J.; Wood, C.M.; Oakley, S.; Ward, S.E. Can digital image classification be used as a standardised method for surveying peatland vegetation cover? *Ecol. Indic.* **2016**, *68*, 150–156. [[CrossRef](#)]
7. Kerkech, M.; Hafiane, A.; Canals, R. Deep leaning approach with colorimetric spaces and vegetation indices for wine diseases detection in UAV images. *Comput. Electron. Agric.* **2018**, *155*, 237–243. [[CrossRef](#)]
8. Wang, Y.; Ziv, G.; Adami, M.; Mitchard, E.; Batterman, S.A.; Buermann, W.; Marimon, B.S.; Junior, B.H.M.; Reis, S.M.; Rodrigues, D.; et al. Mapping tropical disturbed forests using multi-decadal 30 m optical satellite imagery. *Remote Sens. Environ.* **2019**, *221*, 474–488. [[CrossRef](#)]
9. Langner, A.; Miettinen, J.; Siegert, F. Land cover change 2002–2005 in Borneo and the role of fire derived from MODIS imagery. *Glob. Chang. Biol.* **2007**, *13*, 2329–2340. [[CrossRef](#)]
10. Calleja, F.; Ondiviela, B.; Galván, C.; Recio, M.; Juanes, J.A. Mapping estuarine vegetation using satellite imagery: The case of the invasive species *Baccharis halimifolia* at a Natura 2000 site. *Cont. Shelf Res.* **2019**, *174*, 35–47. [[CrossRef](#)]
11. Geerling, G.W.; Labrador-Garcia, M.; Clevers, J.G.P.W.; Ragas, A.M.J.; Smits, A.J.M. Classification of floodplain vegetation by data fusion of spectral (CASI) and LiDAR data. *Int. J. Remote Sens.* **2007**, *28*, 4263–4284. [[CrossRef](#)]
12. Straatsma, M.W.; Baptist, M.J. Floodplain roughness parameterization using airborne laser scanning and spectral remote sensing. *Remote Sens. Environ.* **2008**, *112*, 1062–1080. [[CrossRef](#)]
13. Iersel, W.; Straatsma, M.; Addink, E.; Middelkoop, H. Monitoring height and greenness of non-woody floodplain vegetation with UAV time series. *ISPRS J. Photogramm. Remote Sens.* **2018**, *141*, 112–123. [[CrossRef](#)]
14. Colomina, I.; Molina, P. Unmanned aerial systems for photogrammetry and remote sensing: A review. *ISPRS J. Photogramm. Remote Sens.* **2014**, *92*, 79–97. [[CrossRef](#)]
15. Husson, E.; Reese, H.; Ecke, F. Combining spectral data and a DSM from UAS-images for improved classification of non-submerged aquatic vegetation. *Remote Sens.* **2017**, *9*, 247. [[CrossRef](#)]
16. Senthilnath, J.; Kandukuri, M.; Dokania, A.; Ramesh, K.N. Application of UAV imaging platform for vegetation analysis based on spectral-spatial methods. *Comput. Electron. Agric.* **2017**, *140*, 8–24. [[CrossRef](#)]
17. Huang, Y.; Thomson, S.J.; Hoffmann, W.C.; Lan, Y.; Fritz, B.K. Development and prospect of unmanned aerial vehicle technologies for agricultural production management. *Int. J. Agric. Biol. Eng.* **2013**, *6*, 1–10.
18. Ishida, T.; Kurihara, J.; Viray, F.A.; Namuco, S.B.; Paringit, E.C.; Perez, G.J.; Takajashi, Y.; Marciano, J.J. A novel approach for vegetation classification using UAV-based hyperspectral imaging. *Comput. Electron. Agric.* **2018**, *144*, 80–85. [[CrossRef](#)]
19. Viña, A.; Gitelson, A.A.; Nguy-Robertson, A.L.; Peng, Y. Comparison of different vegetation indices for the remote assessment of green leaf area index of crops. *Remote Sens. Environ.* **2011**, *115*, 3468–3478. [[CrossRef](#)]
20. Dandois, J.P.; Ellis, E.C. High spatial resolution three-dimensional mapping of vegetation spectral dynamics using computer vision. *Remote Sens. Environ.* **2013**, *136*, 259–276. [[CrossRef](#)]
21. Rodriguez, W.; Feller, I.C.; Cavanaugh, K.C. Spatio-temporal changes of a mangrove-saltmarsh ecotone in the northeastern coast of Florida, USA. *Glob. Ecol. Conserv.* **2016**, *7*, 245–261. [[CrossRef](#)]
22. Rusnák, M.; Slaádek, J.; Kidová, A.; Lehotský, M. Template for high-resolution river landscape mapping using UAV technology. *Measurement* **2018**, *115*, 139–151. [[CrossRef](#)]

23. Prošek, J.; Šimová, P. UAV for mapping shrubland vegetation: Does fusion of spectral and vertical information derived from a single sensor increase the classification accuracy? *Int. J. Appl. Earth. Obs. Geoinf.* **2019**, *75*, 151–162. [[CrossRef](#)]
24. Su, J.; Liu, G.; Coombes, M.; Hu, X.; Wang, C.; Xu, X.; Li, Q.; Guo, L.; Chen, W. Wheat yellow rust monitoring by learning from multispectral UAV aerial imagery. *Comput. Electron. Agric.* **2018**, *155*, 157–166. [[CrossRef](#)]
25. Rasmussen, J.; Ntakos, G.; Nielsen, J.; Svendsgaard, J.; Poulsen, R.N.; Christensen, S. Are vegetation indices derived from consumer-grade cameras mounted on UAVs sufficiently reliable for assessing experimental plots? *Eur. J. Agron.* **2016**, *74*, 75–92. [[CrossRef](#)]
26. Agapiou, A.; Hadjimitsis, D.G.; Alexakis, D.D. Evaluation of Broadband and Narrowband Vegetation Indices for the Identification of Archaeological Crop Marks. *Remote Sens.* **2012**, *4*, 3892–3919. [[CrossRef](#)]
27. Hunt, E.R.; Doraiswamy, P.C.; McMurtrey, J.E.; Daughtry, C.S.T.; Perry, E.M.; Akhmedov, B. A visible band index for remote sensing leaf chlorophyll content at the canopy scale. *Int. J. Appl. Earth Obs. Geoinf.* **2013**, *21*, 103–112. [[CrossRef](#)]
28. Martín-Sotoca, J.J.; Saa-Requejo, A.; Borondo, J.; Tarquis, A.M. Singularity maps applied to a vegetation index. *Biosys. Eng.* **2018**, *168*, 42–53. [[CrossRef](#)]
29. Dong, T.; Liu, J.; Shang, J.; Qian, B.; Ma, B.; Kovacs, J.M.; Walters, D.; Jiao, X.; Geng, X.; Shi, Y. Assessment of red-edge vegetation indices for crop leaf area index estimation. *Remote Sens. Environ.* **2019**, *222*, 133–143. [[CrossRef](#)]
30. Song, B.; Oh, J.Y.; Kim, S.S.; Lee, T.W.; Park, K.H. Analysis of 3D Topographic Information on Reservoir Using UAV and Echo Sounder. *J. Disaster Manag.* **2018**, *18*, 563–568. (In Korean) [[CrossRef](#)]
31. Rouse, J.W.; Haas, R.H.; Schell, J.A.; Deering, D.W. Monitoring vegetation systems in the Great Plains with ERTS. In Proceedings of the 3th Earth Resources Technology Satellite-1 Symposium, Goddard Space Flight Center, NASA, Washington, DC, USA, 10–14 December 1973; pp. 309–317.
32. Drone Aerial Mapping and Survey. Available online: <http://www.aeroeye.com.au> (accessed on 10 January 2019).
33. Gitelson, A.; Merzlyak, M.N. Quantitative estimation of chlorophyll-a using reflectance spectra: Experiments with autumn chestnut and maple leaves. *J. Photochem. Photobiol. B* **1994**, *22*, 247–252. [[CrossRef](#)]
34. Pearson, R.L.; Miller, L.D. Remote mapping of standing crop biomass for estimation of the productivity of the shortgrass prairie. In Proceedings of the Eighth International Symposium on Remote Sensing of Environment, University of Michigan, Ann Arbor, MI, USA, 2–6 October 1972; pp. 1357–1381.
35. Gitelson, A.; Kaufman, Y.J.; Merzlyak, M.N. Use of a Green Channel in Remote Sensing of Global Vegetation from EOS-MODIS. *Remote Sens. Environ.* **1996**, *58*, 289–298. [[CrossRef](#)]
36. Jannoura, R.; Brinkmann, K.; Uteau, D.; Bruns, C.; Joergensen, R.G. Monitoring of crop biomass using true colour aerial photographs taken from a remote controlled hexacopter. *Biosys. Eng.* **2015**, *129*, 341–351. [[CrossRef](#)]
37. Elazab, A.; Ordóñez, R.A.; Savin, R.; Slafer, G.A.; Araus, J.L. Detecting interactive effects of N fertilization and heat stress on maize productivity by remote sensing techniques. *Eur. J. Agron.* **2016**, *73*, 11–24. [[CrossRef](#)]
38. Xu, F.; Gao, Z.; Jiang, X.; Shang, W.; Ning, J.; Song, D.; Ai, J. A UAV and S2A data-based estimation of the initial biomass of green algae in the South Yellow Sea. *Mar. Pollut. Bull.* **2018**, *128*, 408–414. [[CrossRef](#)] [[PubMed](#)]
39. Smigaj, M.; Gaulton, R.; Suárez, J.C.; Barr, S.L. Combined use of spectral and structural characteristics for improved red band needle blight detection in pine plantation stands. *For. Ecol. Manag.* **2019**, *434*, 213–223. [[CrossRef](#)]
40. Shimada, S.; Matsumoto, J.; Sekiyama, A.; Aosier, B.; Yokohana, M. A new spectral index to detect Poaceae grass abundance in Mongolian grasslands. *Adv. Space Res.* **2012**, *50*, 1266–1277. [[CrossRef](#)]
41. Li, W.; Niu, Z.; Chen, H.; Li, D.; Wu, M.; Zhao, W. Remote estimation of canopy height and aboveground biomass of maize using high-resolution stereo images from a low-cost unmanned aerial vehicle system. *Ecol. Indic.* **2016**, *67*, 637–648. [[CrossRef](#)]

